Inorganic Chemistry
Article

Proton Reduction and Dihydrogen Oxidation on Models of the [2Fe]$_H$ Cluster of [Fe] Hydrogenases. A Density Functional Theory Investigation

Giuseppe Zampella, Claudio Greco, Piercarlo Fantucci, and Luca De Gioia*

Department of Biotechnology and Biosciences, University of Milano−Bicocca, Piazza della Scienza 1, I-20156 Milan, Italy

Density functional theory was used to compare reaction pathways for H$_2$ formation and H$^+$ reduction catalyzed by models of the binuclear cluster found in the active site of [Fe] hydrogenases. Terminal H$^+$ binding to an Fe^I–Fe^I form, followed by monoelectron reduction and protonation of the di(thiomethyl)amine ligand, can conveniently lead to H$_2$ formation and release, suggesting that this mechanism could be operative within the enzyme active site. However, a pathway that implies the initial formation of Fe^{II}–Fe^{II} μ-H species and release of H$_2$ from an Fe^{II}–Fe^I form is characterized by only slightly less favored energy profiles. In both cases, H$_2$ formation becomes less favored when taking into account the competition between CN and amine groups for H$^+$ binding, an observation that can be relevant for the design of novel synthetic catalysts. H$_2$ cleavage can take place on Fe^{II}–Fe^{II} redox species, in agreement with previous proposals [Fan, H.-J.; Hall, M. B. *J. Am. Chem. Soc.* **2001**, *123*, 3828] and, in complexes characterized by terminal CO groups, does not need the involvement of an external base. The step in H$_2$ oxidation characterized by larger energy barriers corresponds to the second H$^+$ extraction from the cluster, both considering Fe^{II}–Fe^{II} and Fe^{II}–Fe^{III} species. A comparison of the different reaction pathways reveals that H$_2$ formation could involve only Fe^I–Fe^I, Fe^{II}–Fe^I, and Fe^{II}–Fe^{II} species, whereas Fe^{III}–Fe^{II} species might be relevant in H$_2$ cleavage.

Introduction

The development of sustainable ways to produce large amounts of H$_2$ may have great technological relevance soon.[1] Presently, the industrial conversion of protons and electrons to H$_2$ is catalyzed by expensive Pt-containing catalysts.[2] However, enzymes known as hydrogenases contain inexpensive but fundamental Fe and/or Ni ions and can efficiently catalyze the reaction 2H$^+$ + 2e$^-$ → H$_2$,[3] disclosing the potential possibility of using these enzymes and/or bioinspired synthetic catalysts in energy-transduction technology.

Three classes of hydrogenases have been characterized so far. [NiFe] hydrogenases, which contain Ni and Fe ions in the active site, are usually involved in H$_2$ oxidation in vivo; [Fe] hydrogenases, which contain an unusual Fe$_6$S$_6$ moiety (referred to as the H cluster) in their active site, are generally very efficient in H$_2$ production; and another class of Fe-containing hydrogenases for which detailed structural information are still unavailable.[4]

The H cluster in [Fe] hydrogenases is composed of a regular [Fe$_4$S$_4$] cluster bridged by a cysteine residue to a binuclear subcluster ([2Fe]$_H$) where the cleavage of H$_2$ is thought to take place (Chart 1a).[5] The two Fe atoms of [2Fe]$_H$, referred to as distal (Fe1) and proximal (Fe2) with respect to the bridging cysteine residue, are coordinated by CO and CN$^-$ ligands and by a chelating S−X$_3$−S moiety,

* To whom correspondence should be addressed. E-mail: luca.degioia@unimib.it. Fax. +39-02-64483478.

(1) Happe, T.; Hemschemeier, A.; Winkler, M.; Kaminski, A. *Trends Plant Sci.* **2002**, *7*, 246.
(2) Darensbourg, M. Y. *Nature* **2005**, *433*, 589.
(3) Albracht, S. P. *Biochim. Biophys. Acta* **1994**, *167*, 1188. Graf, E. G.; Thauer, R. K. *FEBS Lett.* **1981**, *136*, 165. Adams, M. W. W. *Biochim. Biophys. Acta* **1990**, *115*, 1020. Cammack, R. *Nature* **1999**, *397*, 214. Nicolet, Y.; Lemon, B. J.; Fontecilla-Camps, J. C.; Peters, J. W. *Trends Biochem. Sci.* **2000**, *25*, 138. Peters, J. W. *Curr. Opin. Struct. Biol.* **1999**, *9*, 670. Horner, D. S.; Heil, B.; Happe, T.; Embley, T. M. *Trends Biochem. Sci.* **2002**, *27*, 148. Nicolet, Y.; Cavazza, C.; Fontecilla-Camps, J. C. *J. Inorg. Biochem.* **2002**, *91*, 1. Cammack, R., Frey, M., Robson, R., Eds. *Hydrogen as fuel−Learning from Nature*; Taylor and Francis: London, 2001. Armstrong, F. A. *Curr. Opin. Chem. Biol.* **2004**, *8*, 133.
(4) Lyon, E. J.; Shima, S.; Buurman, G.; Chowdhuri, S.; Batschauer, A.; Steinbach, K.; Thauer, R. K. *Eur. J. Biochem.* **2004**, *271*, 195.
(5) Nicolet, Y.; Piras, C.; Legrand, P.; Hatchikian, E. C.; Fontecilla-Camps, J. C. *Structure* **1999**, *7*, 13. Peters, J. W.; Lanzilotta, W. N.; Lemon, B. J.; Seefeldt, L. C. *Science* **1998**, *282*, 1853.

Scheme 1. Plausible Reaction Pathways for H_2 or H^+ Binding

Path *a*

L = H_2 or H^+

Path *b*
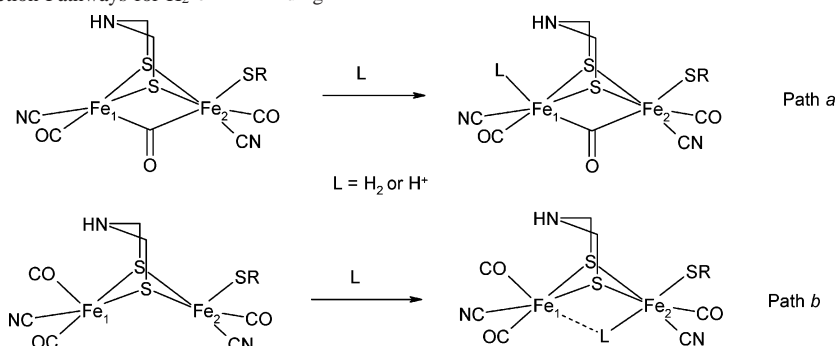
Chart 1. Schematic Structures of the [2Fe]$_H$ Cluster (a) and of a Classical Structural Synthetic Model[9] (b)

a   b
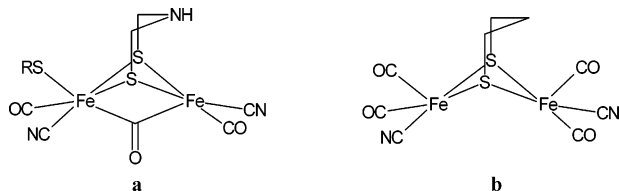
where X_3 is composed of covalently bound light atoms. The nature of the X atoms is still uncertain, and both di-(thiomethyl)amine (DTMA) and 1,3-propanedithiolate (PDT) have been proposed as plausible chelating groups.[5,6]

The peculiar structure of the H cluster in [Fe] hydrogenases has stimulated synthetic studies aimed at a better understanding of structure−activity relationships, with the ultimate goal to design efficient catalysts to be used in H_2 conversion technology.[7,8] Remarkably, most synthetic models are characterized by a vacant binding site between the two Fe centers of the [2Fe]$_H$ cluster, whereas in the enzymatic forms characterized by X-ray diffraction, a CO group bridges the metal centers and the distal Fe is characterized by a vacant binding site (Chart 1).[5]

The origin of the structural difference between the enzyme cofactor and synthetic models has been recently proposed, on the grounds of experimental[6] and density functional theory (DFT)[10] results, to stem from the redox state of the metal

cofactor, as well as from the electronic properties of the Fe ligands. In fact, experimental results are consistent with a scenario where the μ-CO group in the [2Fe]$_H$ cluster moves to a terminal position upon reduction of the enzyme.[6] The latter observations suggest that different H_2 activation/formation pathways are plausible. If a μ-CO group is present in the [2Fe]$_H$ cluster and the chelating group bridging the two Fe centers is assumed to be DTMA, it has been proposed that only the distal Fe center is involved in H_2 or H^+ binding (Scheme 1, path a). In particular, Cao and Hall showed that H_2 cleavage on the Fe1 atom of the $Fe^{II}-Fe^{II}$ complex [(H_2)-$(CO)_2(CN)Fe(\mu$-PDT)Fe(CO)(CN)(MeS)]$^-$ is kinetically or thermodynamically hindered when PDT is the ligand chelating the two Fe centers.[11] When the PDT group is substituted by DTMA, the heterolytic cleavage of H_2 mediated by the N atom of the chelating ligand becomes kinetically favorable.[12] Similar conclusions were reached by Liu and Hu.[13]

Protonation of Fe^I-Fe^I synthetic models of the [2Fe]$_H$ cluster generally takes place at the Fe−Fe bond, suggesting that also μ-H species might be formed along the catalytic cycle (Scheme 1, path b). In fact, Fe2 species bearing a terminal hydride ligand have remained unknown until very recently, when Rauchfuss and collaborators reported the characterization of [Fe$_2$(edt)(μ-CO)(H)(CO)(PMe$_3$)$_4$]PF$_6$, which slowly rearranges to the corresponding μ-H isomer.[14] Moreover, DFT calculations indicate that if the μ-CO group moves to a terminal position, H_2 can bind to the proximal Fe center.[15] In particular, Bruschi et al. have investigated H_2 binding and activation on the model system [(CO)$_2$(CN)Fe-(μ-PDT)Fe(CO)(CN)(CH$_3$S)]$^-$, taking into account the possible involvement of μ-H intermediate species.[16] It turned out that H_2 binds to Fe2, and it can undergo heterolytic cleavage resulting in coordination of H^- to both metal centers. Zhou et al. recently reached very similar conclusions,[17] suggesting that H_2 activation in the enzyme involves both Fe centers. The observation that H_2 activation/formation might follow different reaction routes can also be relevant for the design of synthetic catalysts. In fact, despite brilliant

(6) Nicolet, Y.; de Lacey, A. L.; Vernede, X.; Fernandez, V. M.; Hatchikian, E. C.; Fontecilla-Camps, J. C. *J. Am. Chem. Soc.* **2001**, *123*, 1596.

(7) Evans, D. J.; Pickett, C. J. *Chem. Soc. Rev.* **2003**, *35*, 268. Rauchfuss, T. B. *Inorg. Chem.* **2004**, *43*, 14. Darensbourg, M. Y.; Lyon, E. J.; Smee, J. J. *Coord. Chem. Rev.* **2000**, *206−207*, 533.

(8) Georgakaki, I. P.; Miller, M. L.; Darensbourg, M. Y. *Inorg. Chem.* **2003**, *42*, 2489. Zhao, X.; Georgakaki, I. P.; Miller, M. L.; Yarbrouch, J. C.; Darensbourg, M. Y. *J. Am. Chem. Soc.* **2001**, *123*, 9710. Boyke, C. A.; Rauchfuss, T. B.; Wilson, S. R.; Rohmer, M.-M.; Benard, M. *J. Am. Chem. Soc.* **2004**, *126*, 15151. Rauchfuss, T. B. *Inorg. Chem.* **2004**, *43*, 14. Evans, D. J.; Pickett, C. J. *Chem. Soc. Rev.* **2003**, *32*, 268. Razavet, M.; Davies, S. C.; Hughes, D. L.; Barclay, J. E.; Evans, D. J.; Fairhurst, S. A.; Liu, X.; Pickett, C. J. *J. Chem. Soc., Dalton Trans.* **2003**, 586. Borg, S. J.; Behrsing, T.; Best, S. P.; Razavet, M.; Liu, X.; Pickett, C. J. *J. Am. Chem. Soc.* **2004**, 126, 16988. Song, L.-C.; Yang, Z.-Y.; Bian, H.-Z.; Hu, Q.-M. *Organometallics* **2004**, *23*, 3082. Lee, C.-M.; Chen, C.-H.; Ke, S.-C.; Lee, G. H.; Liaw, W.-F. *J. Am. Chem. Soc.* **2004**, *126*, 8406.

(9) Lyon, E. J.; Georgakaki, I. P.; Reibenspies, J. H.; Darensbourg, M. Y. *Angew. Chem., Int. Ed.* **1999**, *38*, 3178. Le Cloirec, A.; Best, S. P.; Borg, S.; Davies, S. C.; Evans, D. J.; Hughes, D. L.; Pickett, C. J. *Chem. Commun.* **1999**, 2285. Schmidt, M.; Contakes, S. M.; Rauchfuss, T. B. *J. Am. Chem. Soc.* **1999**, *121*, 9736.

(10) Bruschi, M.; Fantucci, P.; De Gioia, L. *Inorg. Chem.* **2004**, *43*, 3733.

(11) Cao, Z.; Hall, M. B. *J. Am. Chem. Soc.* **2001**, *123*, 3734.

(12) Fan, H.-J.; Hall, M. B. *J. Am. Chem. Soc.* **2001**, *123*, 3828.

(13) Liu, Z.-P.; Hu, P. *J. Am. Chem. Soc.* **2002**, *124*, 5175.

(14) Van der Vlugt, J. I.; Rauchfuss, T. B.; Whaley, C. M.; Wilson, S. R. *J. Am. Chem. Soc.* **2005**, *127*, 16012.

(15) Bruschi, M.; Fantucci, P.; De Gioia, L. *Inorg. Chem.* **2003**, *42*, 4773.

(16) Bruschi, M.; Fantucci, P.; De Gioia, L. *Inorg. Chem.* **2002**, *41*, 1421.

(17) Zhou, T.; Mo, Y.; Liu, A.; Zhou, Z.; Tsai, K. R. *Inorg. Chem.* **2004**, *43*, 923.

results obtained by synthetic chemists, the catalytic activity of the enzyme is still orders of magnitude larger than that reported for synthetic models.

Other theoretical investigations of models of the [2Fe]$_H$ cluster have been recently reported,[18−21] disclosing relevant structure−activity relationships and showing once again that quantum chemical studies can nicely complement experimental investigations in the characterization of metal-containing enzymes and related synthetic complexes.[22−24]

With the aim of contributing to the clarification of the chemical factors more relevant for catalysis and shedding light on the peculiar reactivity properties of the *isolated* [2Fe]$_H$ cluster and related models, we have used DFT to characterize and compare H$^+$ reduction and H$_2$ oxidation pathways (Scheme 1, paths a and b). In fact, most DFT studies reported so far were confined to the investigation of the H$_2$ cleavage/formation step, along either path a or path b, precluding a direct comparison of the two pathways. Moreover, other relevant steps in the catalytic cycle, such as H$^+$ binding to the [2Fe]$_H$ cluster, have received relatively little attention.

In the first section of the paper, results related to the protonation of Fe^I−Fe^I and Fe^{II}−Fe^I models of the [2Fe]$_H$ cluster are presented and discussed. In the second section, structures and reaction energy profiles relevant for H$_2$ production/cleavage are presented. To evaluate possible environmental effects, free-energy values have been computed both in a vacuum and by soaking the complexes in a polarizable continuum medium (COSMO approach)[25] characterized by dielectric constant values commonly used to model proteins ($\epsilon = 4$ and 40).[26] In the final section, the relevance of the present results for the elucidation of the catalytic mechanism of [Fe] hydrogenases and for the design of novel synthetic catalysts is discussed.

Methods

Calculations have been carried out with the TURBOMOLE 5.7 suite,[27] applying the resolution-of-the-identity technique[28] in order to speed up calculations.

Geometry optimizations and transition-state searches have been carried out using the pure functional BP86,[29] as implemented in TURBOMOLE, in conjunction with a valence triple-ζ basis set with polarization on all atoms (TZVP),[30] a level of theory that has been shown to be suitable to reliably investigate [Fe] hydrogenase models.[18,20,21]

A restricted framework was employed for closed-shell electronic structures, whereas unrestricted Kohn−Sham calculations were carried out for open-shell complexes. In light of the available experimental data and considering the chemical nature of the ligands, only low-spin species have been investigated.

Stationary points of the energy hypersurface have been located by means of energy-gradient techniques, and full vibrational analysis has been carried out to further characterize each stationary point. Relevant IR bands, computed for all intermediate species, are available as Supporting Information.

The optimization of transition-state structures has been carried out according to a procedure based on a pseudo-Newton−Raphson method. Initially, geometry optimization of a guessed transition-state structure is carried out by constraining the distance corresponding to the reaction coordinate. Vibrational analysis at the BP86/TZVP level of the constrained minimum-energy structures is then carried out, and if one negative eigenmode corresponding to the reaction coordinate is found, the curvature determined at such a point is used as the starting point in the transition-state search. The location of the transition-state structure is carried out using an eigenvector-following search: the eigenvectors in the Hessian are sorted in ascending order, with the first one being that associated with the negative eigenvalue. After the first step, however, the search is performed by choosing the critical eigenvector with a maximum overlap criterion, which is based on the dot product with the eigenvector followed in the previous step.
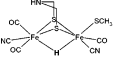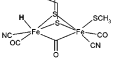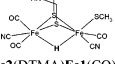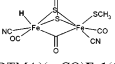
Free-energy (G) values have been obtained from the electronic self-consistent-field (SCF) energy considering three contributions to the total partition function (Q), namely, $q_{\text{translational}}$, $q_{\text{rotational}}$, and $q_{\text{vibrational}}$, under the assumption that Q may be written as the product of such terms.[31] To evaluate enthalpy and entropy contributions, the values for temperature and pressure have been set to 298.15 K and 1 bar, respectively. The scaling factor for the SCF wavenumbers was set either to 0.9 (default value in the TURBOMOLE script FREEH, by means of which thermodynamics corrections are computed) or 0.9914 (a value usually applied with the BP86 functional).[32] It turned out that computed ΔG values change by less than 0.5 kcal mol^{-1} upon switching from 0.9 to 0.9914. Rotations have been treated classically, and vibrational modes have been described according to the harmonic approximation.

Effects due to the proteic environment have been simply modeled according to the COSMO approach.[25] In particular, to better evaluate environmental effects, calculations have been carried out both in a vacuum ($\epsilon = 1$) and by considering a polarizable continuum medium characterized by two different ϵ values ($\epsilon = 4$ and 40) that are commonly used to model proteins.[26]

H$^+$ binding energy values have been computed as the free-energy difference in the reaction M + H$^+$ → MH$^+$, where M is the

(18) Zampella, G.; Bruschi, M.; Fantucci, P.; Razavet, M.; Pickett, C. J.; De Gioia, L. *Chem.−Eur. J.* **2005**, *11*, 509.

(19) Georgakaki, I. P.; Thomson, L. M.; Lyon, E. J.; Hall, M. B.; Darensbourg, M. Y. *Coord. Chem. Rev.* **2003**, *238−239*, 255.

(20) Tard, C.; Liu, X.; Ibrahim, S. K.; Bruschi, M.; De Gioia, L.; Davies, S. C.; Yang, X.; Wang, L.-S.; Sawers G.; Pickett, C. J. *Nature* **2005**, *433*, 610.

(21) Boyke, C. A.; van der Vlugt, J. I.; Rauchfuss, T. B.; Wilson, S. R.; Zampella, G.; De Gioia, L. *J. Am. Chem. Soc.* **2005**, *127*, 11010.

(22) Niu, S.; Hall, M. B. *Chem. Rev.* **2000**, *100*, 353. Siegbahn, P. E. M.; Blomberg, M. R. A. *Chem. Rev.* **2000**, *100*, 421. Lovell, T.; Himo, F.; Han, W.-G.; Noodleman, L. *Coord. Chem. Rev.* **2003**, *238−239*, 211. Friesner, R. A.; Baik, M.-H.; Gherman, B. F.; Guallar, V.; Wirstam, M.; Murphy, R. B.; Lippard S. J. *Coord. Chem. Rev.* **2003**, *238−239*, 267.

(23) Stein, M.; Lubitz, W. *Curr. Opin. Chem. Biol.* **2002**, *6*, 243.

(24) Ziegler, T.; Autschbach, J. *Chem. Rev.* **2005**, *105*, 2695.

(25) Klamt, A. *J. Phys. Chem.* **1995**, *99*, 2224. Klamt A. *J. Phys. Chem.* **1996**, *100*, 3349.

(26) Himo, F.; Noodleman, L.; Blomberg, M. R. A.; Siegbahn, P. E. M. *J. Phys. Chem. A* **2002**, *106*, 8757. Klamnt, A. *J. Phys. Chem.* **1995**, *99*, 2224. Klamnt A. *J. Phys. Chem*. **1996**, *100*, 3349. Warshel, A.; Naray-Szabo, G.; Sussman, F.; Hwang, J.-K. *Biochemistry* **1989**, *28*, 3629. Bottoni, A.; Lanza, C. Z.; Miscione, G. P.; Spinelli, D. *J. Am. Chem. Soc.* **2004**, *126*, 1542−1550.

(27) Ahlrichs, R.; Bar, M.; Haser, M.; Horn, H.; Kolmel, C. *Chem. Phys. Lett.* **1989**, *162*, 165.

(28) Eichkorn, K.; Weigend, F.; Treutler, O.; Ahlrichs, R. *Theor. Chem. Acc.* **1997**, *97*, 119.

(29) Becke, A. D. *Phys. Rev. A* **1988**, *38*, 3098. Perdew, J. P. *Phys. Rev. B* **1986**, *33*, 8822.

(30) Schafer, A.; Huber, C.; Ahlrichs, R. *J. Chem. Phys.* **1994**, *100*, 5829.

(31) Jensen, F. *Introduction to Computational Chemistry*; John Wiley & Sons Ltd.: Chichester, England, 2002.

(32) Cramer, C. J. *Essentials of computational chemistry−Theories and models*; Wiley: New York, 2002.

Table 1. Computed Free Energies Differences (in kcal mol^{-1}) for the Reaction M + H$^+$ → MH$^+$, Where M Are Fe^I–Fe^I and Fe^{II}–Fe^I Models of the [2Fe]$_H$ Cluster[a]

Complex	ΔG ($\epsilon=1$)	ΔG ($\epsilon=4$)	ΔG ($\epsilon=40$)
[(CH$_3$S)**Fe2**(DTMA)**Fe1**(CO)$_2$(CN)$_2$]$^{3-}$ {Fe(I)Fe(I)}	-476.9	-358.9	-305.7
[(CH$_3$S)**Fe2**(DTMA)(μ-CO)**Fe1**(CO)$_2$(CN)$_2$]$^{3-}$ {Fe(I)Fe(I)}	-466.4	-347.2	-293.4
[(CH$_3$S)**Fe2**(DTMA)**Fe1**(CO)$_2$(CN)$_2$]$^{2-}$ {Fe(II)Fe(I)}	-384.5	-314.3	-282.7
[(CH$_3$S)**Fe2**(DTMA)(μ-CO)**Fe1**(CO)$_2$(CN)$_2$]$^{2-}$ {Fe(II)Fe(I)}	-381.7	-310.0	-277.7

[a] The protonation sites are highlighted in boldface. The formal oxidation state of the Fe ions in M is reported as a reference.

binuclear cluster under investigation. Both M and MH$^+$ energies refer to the fully optimized complexes.

Results and Discussion

H$^+$ Binding to Fe^I–Fe^I and Fe^{II}–Fe^I Models of the [2Fe]$_H$ Cluster. H$^+$ binding energy values have been computed in order to evaluate the relative basicity of different sites in the Fe^I–Fe^I and Fe^{II}–Fe^I redox states of the [2Fe]$_H$ models [Fe$_2$(DTMA)(CO)$_3$(CN)$_2$CH$_3$S]$^{3-}$ and [Fe$_2$(DTMA)-(CO)$_3$(CN)$_2$CH$_3$S]$^{2-}$. In fact, the X-ray structure of the enzyme suggests that Fe1 could be the site of protonation,[5] whereas experimental data obtained by studying Fe^I–Fe^I synthetic complexes are generally consistent with the formation of μ-H species.[33] Indeed, it has been recently shown that the regiochemistry of protonation of functional models of the [2Fe]$_H$ cluster can be affected by the chemical properties of coligands,[34] leading to the conclusion that the prediction of the protonation sites in this class of complexes is nontrivial.

It turns out that the lowest ΔG value for the reaction between the Fe^I–Fe^I complex [Fe$_2$(DTMA)(CO)$_3$(CN)$_2$C-H$_3$S]$^{3-}$ and H$^+$ corresponds to the formation of the μ-H adduct (Table 1), while protonation of the distal Fe is less exergonic by more than 10 kcal mol^{-1}. Therefore, our results suggest that, when considering the *isolated* [2Fe]$_H$ cluster, the first step toward H$_2$ production could be the formation of a μ-H intermediate.

A comparison of the relative H$^+$ binding energy values computed for the Fe^{II}–Fe^I complex [Fe$_2$(DTMA)(CO)$_3$(CN)$_2$-CH$_3$S]$^{2-}$ shows that formation of a μ-H species is still more favored than protonation of Fe1 on the μ-CO isomer. However, the energy gap between the two tautomers is smaller for Fe^{II}–Fe^I than for Fe^I–Fe^I species (Table 1).

(33) Le Borgne, G.; Grandjean, D.; Mathieu, R.; Poilblanc, R. *J. Organomet. Chem.* **1977**, *131*, 429. Zhao, X.; Georgakaki, I. P.; Miller, M. L.; Yarbrough, J. C.; Darensbourg, M. Y. *J. Am. Chem. Soc.* **2001**, *123*, 9710.
(34) Gloaguen, F.; Lawrence, J. D.; Rauchfuss, T. B.; Benard, M.; Rohmer, M.-M. *Inorg. Chem.* **2002**, *41*, 6573.

H$_2$ formation on the [2Fe]$_H$ cluster in [Fe] hydrogenases can, at least in principle, take place according to different reaction pathways (Scheme 1). Indeed, even if a mechanism for H$_2$ formation that implies the involvement of the Fe1 center and DTMA fits nicely with the available results, the evidences for the presence of DTMA in the enzyme active site are only indirect and other H$_2$ activation pathways might be operative in the enzyme.[15,17,35] The investigation of alternative routes to H$_2$ formation is also relevant to better understand the chemistry of synthetic models characterized by a vacant coordination position along the Fe–Fe axis and possibly drive the design of new catalysts. In fact, our present study confirms that the Fe–Fe bond is the most basic site of the *isolated* [2Fe]$_H$ cluster. Notably, the involvement of μ-H species in the protein active site might imply the presence of a proton channel connecting the Fe–Fe bond with the protein surface. The analysis of the structure of the enzyme active site reveals that the amine group of a lysine residue (Lys237 in DdHase), which is extremely conserved in [Fe] hydrogenases (not shown), is involved in a H-bonding interaction with a CN group of the [2Fe]$_H$ cluster and might shuttle protons from the protein surface to the bimetallic center.
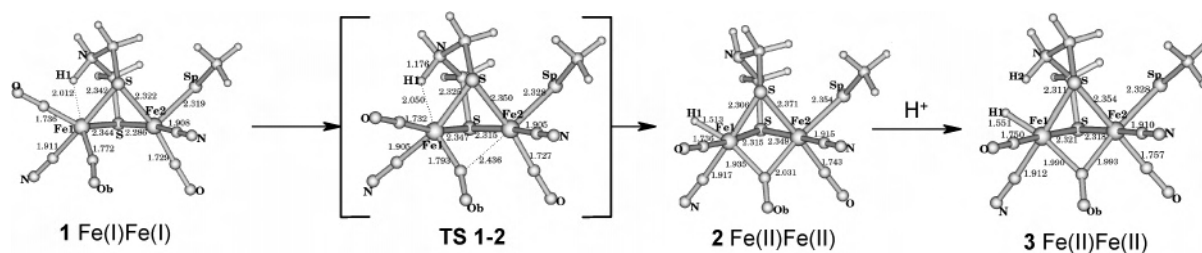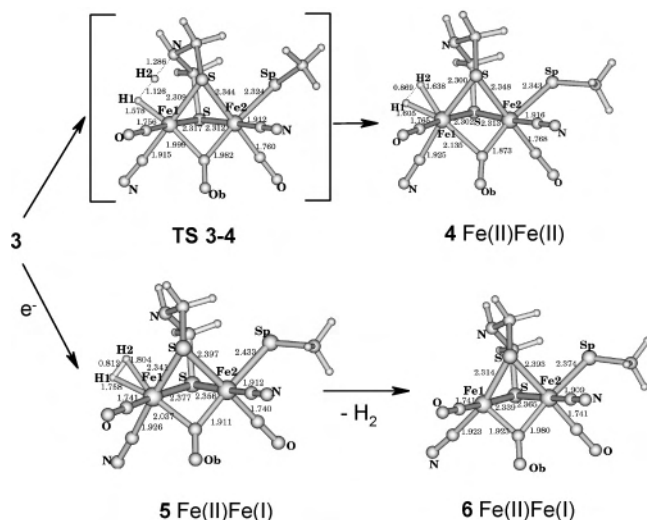
H$_2$ Production Involving H$^+$ Binding to Fe1. In light of the X-ray structure of the [2Fe]$_H$ cluster in the enzyme and assuming that DTMA is the ligand chelating the two Fe atoms, a plausible path for H$_2$ production (Scheme 1, path a) could initially imply H$^+$ binding to the Fe1 atom of the Fe^I–Fe^I form of the model [Fe$_2$(DTMA)(CO)$_3$(CN)$_2$CH$_3$S]$^{3-}$. H$^+$ transfer from the environment to the Fe$_2$S$_3$ cluster could take place via the NH group of the chelating DTMA ligand. In fact, H$^+$ transfer from the NH$_2$$^+$ group of DTMA to Fe1 (**1** → **TS1-2** → **2**; Figure 1) is almost barrierless (ΔG^+ = 2.8, 1.1, and 0.7 kcal mol^{-1} when ϵ = 1, 4, and 40, respectively) and thermodynamically favored (ΔG = −15.6, −9.5, and −4.7 kcal mol^{-1} when ϵ = 1, 4, and 40, respectively). In **1**, one of the CO groups coordinated to Fe1 is bent and weakly interacts with the Fe2 center. Moreover, the distance between the NH$_2$$^+$ group of DTMA and Fe1 is short (2.012 Å). The transition-state structure **TS1-2** has a pronounced reactant-like character, even if the semibridging CO approaches the Fe2 center. In **2**, the CO group is almost symmetrically bound in a μ fashion and the H–Fe1 distance is 1.513 Å.

Protonation of the DTMA group in the Fe^{II}–Fe^{II} species **2** leads to **3**, in which the μ-CO group remains symmetrically bridged and a nonclassical H bond between the H atom coordinated to Fe1 and the NH$_2$$^+$ group of DTMA is formed (Figure 1), in agreement with previous observations reported by Fan and Hall.[12] Species **3** can evolve to **4**, where H$_2$ is already formed and coordinated to Fe1, going through the transition-state structure **TS3-4** (Figure 2). The conversion of **3** → **4** is slightly endergonic when $\epsilon \geq 4$ (ΔG = −5.6, +2.6, and +7.7 kcal mol^{-1} when ϵ = 1, 4, and 40, respectively), and the corresponding activation free energy

(35) In this study no attempt has been made to evaluate the reduction potential of the various complexes, i.e., the reaction energies related to redox steps.

Figure 1. DFT structures (and formal oxidation states) of intermediates and transition states (in square brackets) of species relevant to the reaction path a (see Scheme 1).

Figure 2. DFT structures (and formal oxidation states) of intermediates and transition states (in square brackets) of species relevant to the reaction path a (see Scheme 1).

is less than 0.5 kcal mol^{-1} larger than the free-energy difference when $\epsilon \geq 4$ ($\Delta G^{\ddagger} = 0.5$, 2.8, and 7.8 kcal mol^{-1} when $\epsilon = 1$, 4, and 40, respectively). In **TS3-4**, the transferring H atom is almost equidistant from the N atom of DTMA and the H atom coordinated to Fe1. In **4**, the μ-CO group is closer to the Fe2 center and the H–H distance is 0.869 Å, indicating that the H$_2$ molecule is activated. The observation that a more polar environment disfavors this reaction step can be rationalized in light of the zwitterionic character of the reactant (**3**), where the positively charged NH$_2^+$ moiety interacts with the anionic Fe$_2$S$_3$ cluster.

Notably, if the Fe^{II}–Fe^{II} species **3** undergoes monoelectron reduction,[36] the formation of H$_2$ becomes thermodynamically favored and barrierless; i.e., the Fe^{II}–Fe^{I} species characterized by the simultaneous presence of an H atom coordinated to Fe1 and the NH$_2^+$ group of protonated DTMA does not correspond to an energy minimum and evolves directly toward the Fe1–H$_2$ adduct **5** (Figure 2). In **5**, the H–H distance is shorter (0.812 Å) than that in **4** and the μ-CO group is slightly closer to the Fe2 center. Remarkably, **5** spontaneously releases H$_2$ ($\Delta G = -13.6$, -12.8, and -12.3 kcal mol^{-1} when $\epsilon = 1$, 4, and 40, respectively), leading to the Fe^{II}–Fe^{I} species **6**, where the Fe1 center has a regular square-pyramidal geometry and μ-CO is symmetrically bridged.

(36) Cohen, J.; Kim, K.; Posewitz, M.; Ghirardi, M. L.; Schulten, K.; Seibert, M.; King, P. *Biochem. Soc. Trans.* **2005**, *33*, 80.

Protonation of the DTMA group in **6** leads to **7**, where one CN group has moved from its initial position and interacts with the NH$_2^+$ group of protonated DTMA (Figure 3). The observed movement of the CN group could be hindered in the enzyme active site, where the CN groups are involved in H-bonding interactions with the protein matrix.[5] Monoelectron reduction of species **7** leads to the parent complex **1**. It is worth noting that species **7** could also interconvert to the Fe^{II}–Fe^{III} complex **8** (**7** → **TS7-8** → **8**; Figure 3), in which a H$^+$ has moved from the DTMA ligand to the Fe1 center ($\Delta G = -11.2$, -4.7, and 0.0 kcal mol^{-1} when $\epsilon = 1$, 4, and 40, respectively). In **8**, the NH group of DTMA weakly interacts with the H atom coordinated to Fe1 and the μ-CO group is asymmetrically bound to the cluster, being closer to Fe1 (Figure 3). The conversion from **7** to **8** is characterized by a relatively high activation barrier ($\Delta G^{\ddagger} = 7.9$, 11.6, and 14.5 kcal mol^{-1} when $\epsilon = 1$, 4, and 40, respectively), suggesting that H$^+$ transfer from DTMA to Fe1 could be kinetically hindered when considering the Fe^{II}–Fe^{I} redox state. Moreover, computed ΔG and $\Delta G^{\ddagger}$ values indicate that the environment can significantly affect the reaction energy profile for this reaction step. In particular, a nonpolar environment favors the reaction because of destabilization of the zwitterionic reactant **7**.

To make the comparison between paths a and b fully consistent (see below), we have also investigated path a using a model system where the [2Fe]$_H$ cluster interacts with a lysine residue (here modeled as butylamine/butylammonium) spatially placed according to the position of Lys237 in the enzyme. Indeed, even if the lysine side chain cannot play a direct role in H$_2$ formation according to path a, its presence could subtly influence the geometries and relative stabilities of intermediate species and transition states. In fact, the conversion **1** → **2** becomes barrierless when using the extended model system. Moreover, the presence of the lysine side chain slightly affects geometries of intermediates **2** and **8** (**2-buNH$_2$** and **8-buNH$_2$**; Figure 4), whereas the structures and relative stabilities for all other species are essentially unaffected.

In summary, the above results indicate that initial H$^+$ binding to the Fe1 atom of an Fe^I–Fe^I form, followed by monoelectron reduction and protonation of the DTMA ligand, can conveniently lead to H$_2$ formation and release, suggesting that this reaction pathway could be operative within the enzyme active site. However, if results are discussed in light of possible suggestions for the design of novel synthetic catalysts, it should be noted that further protonation of the
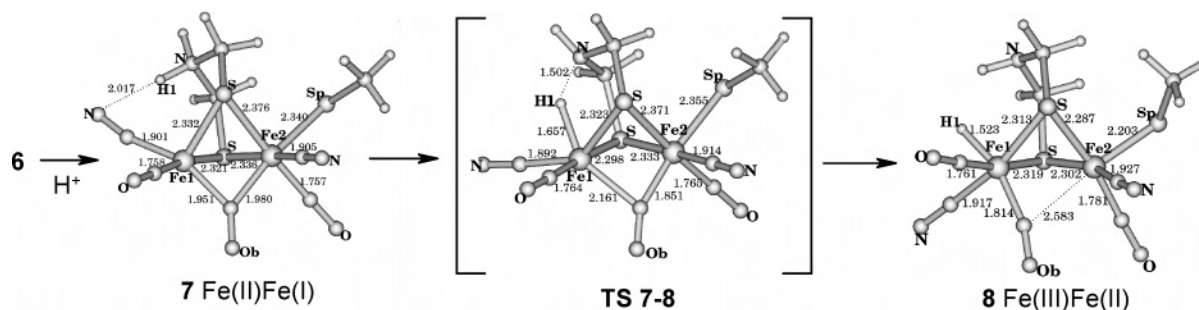
Figure 3. DFT structures (and formal oxidation states) of intermediates and transition states (in square brackets) of species relevant to the reaction path a (see Scheme 1).
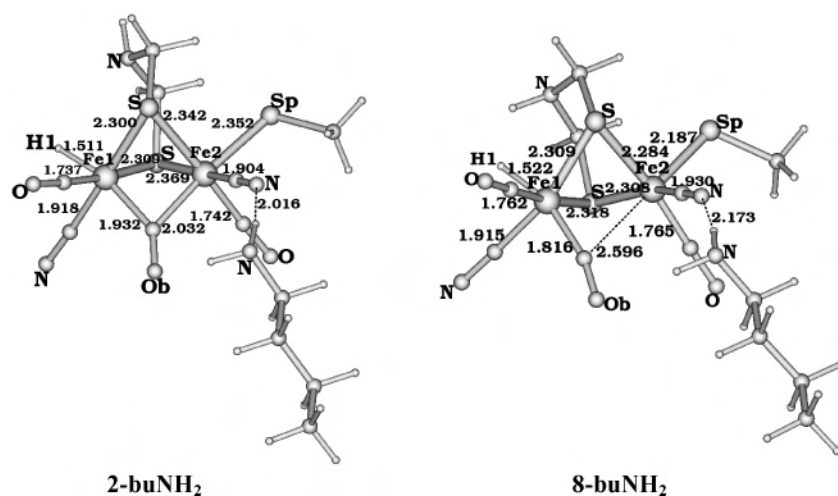
Figure 4. DFT structures of intermediate species **2-buNH₂** and **8-buNH₂**, which differ from **2** and **8** by the presence of a butylamine group placed according to the position of the Lys237 side chain in the enzyme.

*isolated* Fe^{II}–Fe^{I} complex [(μ-H)Fe₂(DTMA)(CO)₃(C-N)₂CH₃S]$^{3-}$ is predicted to take place more easily on the CN groups than on the DTMA ligand (data not shown). As a consequence, the formation of H₂ should take place on the species [(μ-H)Fe₂DTMA(CO)₃(CNH)₂CH₃S]$^{-}$. To evaluate to what extent protonation of the CN groups can affect the energy profile in the H₂ formation step, we have also computed reaction energies and the transition-state structure along the pathway **3′ → 5′**, where **3′** and **5′** (structures not shown) differ from **3** and **5** only for the protonation state of the CN groups. Differently from **3**, monoelectron reduction of **3′** results in a stable Fe^{II}–Fe^{I} intermediate species in which a H atom is coordinated to Fe1 and the other H atom is still bound to the N atom of DTMA (**3″**, not shown). The conversion **3″ → 5′** is characterized by ΔG = −5.6, −1.5, and 1.1 kcal mol^{-1} and ΔG‡ = 0.2, 0.2, and 0.7 kcal mol^{-1} when ε = 1, 4, and 40, respectively. Therefore, protonation of the CN groups decreases the catalytic efficiency of the complex in the H₂ production step, in agreement with the observation made by Rauchfuss and co-workers about the role of electron donor ligands in modulating the activity of complexes capable of catalyzing H^{+} reduction.[34]

H₂ Production Involving H^{+} Binding to Fe1 and Fe2 (μ Fashion). Prompted by the observation that a lysine residue (Lys237) might be involved in H^{+} transfer (see above), we have studied H₂ formation on the [Fe₂(DTMA)-(CO)₃(CN)₂CH₃S]$^{3-}$ model of the [2Fe]$_{H}$ cluster according to a mechanism that implies the formation of μ-H intermediate species (Scheme 1, path b).

The structure of the adduct (**9**) between butylammonium and the Fe^{I}–Fe^{I} form of the [Fe₂(DTMA)(CO)₃(CN)₂CH₃S]$^{3-}$ model, which is characterized by the absence of a μ-CO group, is shown in Figure 5. In **9**, H^{+} transfer from the ammonium group to the Fe^{I}–Fe^{I} cluster leads to the Fe^{II}–Fe^{II} species **10**, where a H atom bridges the two Fe ions (Figure 5). The conversion **9 → 10** is thermodynamically and kinetically facile (ΔG = −24.0, −18.0, and −15.4 kcal mol^{-1} and ΔG‡ = 1.1, 3.5, and 4.6 kcal mol^{-1} when ε = 1, 4, and 40, respectively).[37] In **TS9-10**, the transferring H atom is closer to Fe2 (1.861 Å) than to Fe1, whereas in **10**, the H atom bridges, even if asymmetrically (Fe–H distances = 1.646 and 1.724 Å), the two Fe centers.

---

(37) It should be noted that that the starting position of butylamine in the complexes was always chosen to be consistent with the spatial disposition of the corresponding lysine side chain in the enzyme. However, no constraints were applied to the butylamine group during geometry optimization. In fact, the rearrangement of the butylamine residue during optimization is usually small. Moreover, even when the geometry of the lysine model changes drastically during optimization, the overall reaction profile does not change significantly when compared to the corresponding results obtained by freezing the position of the butylamine C atom corresponding to the C$_{α}$ atom of the lysine amino acid to the corresponding position observed in the enzyme. As an example, the ΔG and ΔG‡ values for the conversion **13 → 14**, which is characterized by drastic rearrangement of the butylamine residue, change consistently by less than 3 kcal mol^{-1}, an energy difference that does not affect our conclusions.
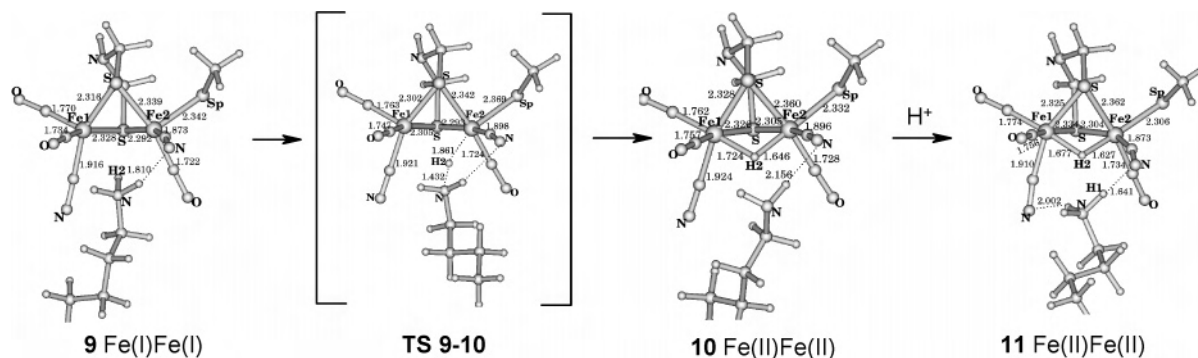
Figure 5. DFT structures (and formal oxidation states) of intermediates and transition states (in square brackets) of species relevant to the reaction path b (see Scheme 1).
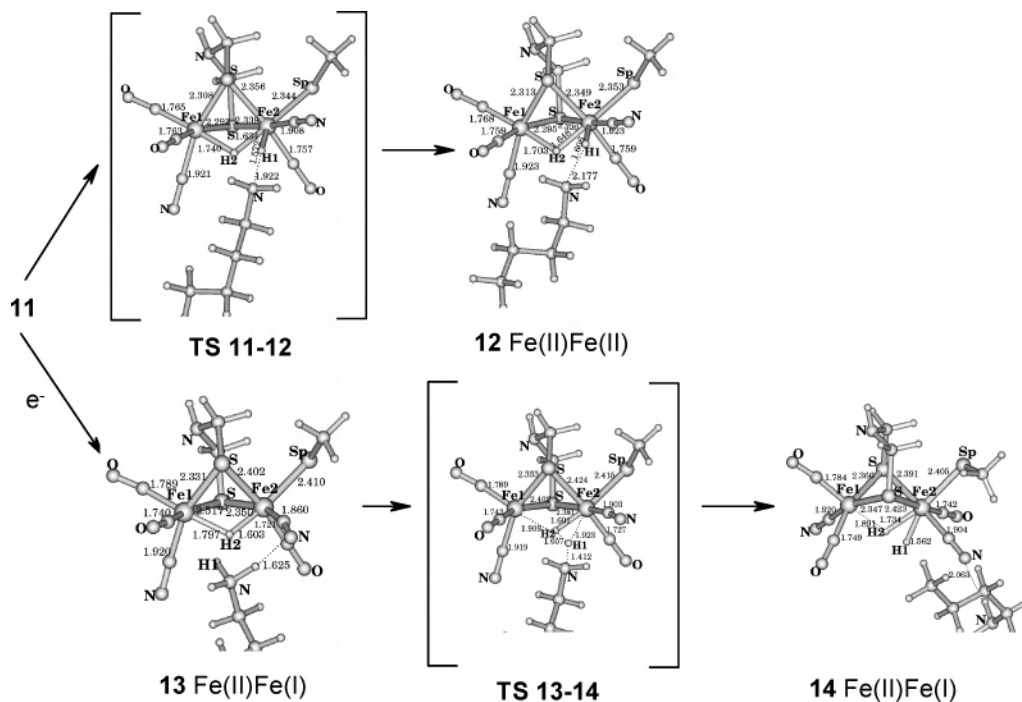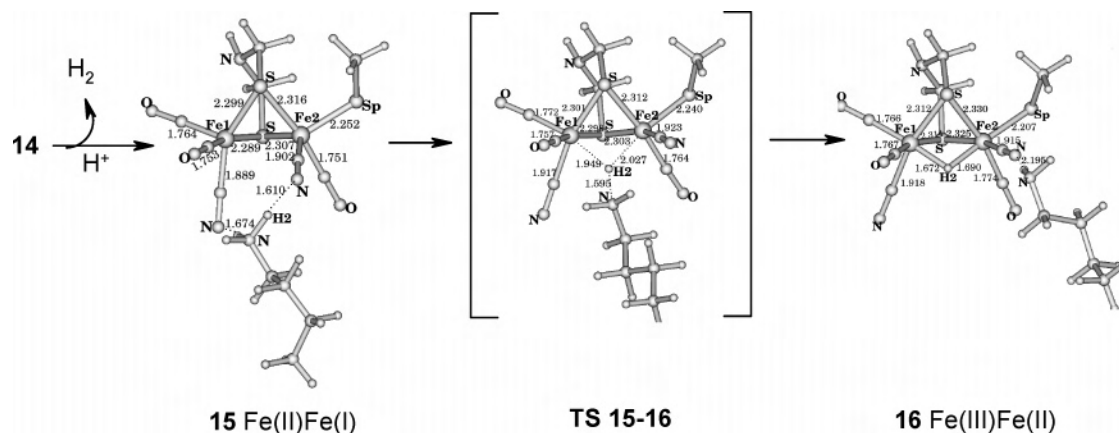

Figure 6. DFT structures (and formal oxidation states) of intermediates and transition states (in square brackets) of species relevant to the reaction path b (see Scheme 1).

Further protonation of butylamine leads to **11**, where the μ-H atom is symmetrically bridged. The transfer of a H$^+$ from butylamonium to the Fe$_2$S$_3$ cluster in **11** leads to the intermediate species **12** (Figure 6), where the transferred H atom is bound to Fe2 and the H—H distance (1.604 Å) is compatible with a cleaved H$_2$ molecule. The corresponding transition-state structure (**TS11-12**) has a pronounced product-like nature. The conversion **11** → **12** is strongly endergonic (ΔG = 14.8, 18.0, and 20.5 kcal mol^{-1} when ϵ = 1, 4, and 40, respectively), suggesting that this reaction pathway is hindered. Notably, the endergonicity of the **11** → **12** step is partly due to the strong H bonds between butylammonium and the CN groups of the anionic cluster, which are lost in **12**.

The Fe^{II}—Fe^{II} species **11** could also follow a different reaction pathway and undergo monoelectron reduction, leading to the Fe^{II}—Fe^{I} species **13** (Figure 6), in which the μ-H atom has a strong asymmetric character, being almost 0.2 Å closer to Fe2 than to Fe1. The intermediate species **13** can evolve to **14**, in which H$_2$ is still activated (H—H

distance = 0.939 Å) and coordinated to Fe2, even though one of the H atoms interacts with Fe1. The H$_2$ formation step taking place on the Fe^{II}—Fe^{I} species **13** is thermodynamically favored when ϵ < 40 (ΔG = −13.2, −3.1, and +1.5 kcal mol^{-1} when ϵ = 1, 4, and 40, respectively). A strongly polar environment leads to a thermodynamically slightly disfavored reaction step due to overstabilization of the reactant (**13**), which can be described as an ion pair between butylammonium and the anionic Fe$_2$S$_3$ cluster. The corresponding computed activation free energies (**13** → **TS13-14**; Figure 6) are 3.6, 7.8, and 9.7 kcal mol^{-1} when ϵ = 1, 4, and 40, respectively, indicating that H$_2$ formation on an Fe^{II}—Fe^{I} species can take place quite easily in a weakly polar environment. H$_2$ release from **14** is strongly exergonic (ΔG = −17.5, −20.7, and −22.9 kcal mol^{-1} when ϵ = 1, 4, and 40, respectively), and protonation of the resulting Fe^{II}—Fe^{I} species leads to **15** (Figure 7), in which the two Fe centers have a distorted square-planar geometry and the vacant coordination sites are along the Fe—Fe axis. H$^+$ transfer from butylammonium to the Fe—Fe moiety **15** could

Figure 7. DFT structures (and formal oxidation states) of intermediates and transition states (in square brackets) of species relevant to the reaction path b (see Scheme 1).

lead to a μ-H $Fe^{II}-Fe^{III}$ species (**16**; Figure 7). However, this reaction step is kinetically hindered ($\Delta G^{\ddagger} = 17.7$, 21.4, and 23.2 kcal mol^{-1} and $\Delta G = 2.9$, 6.2, and 7.1 kcal mol^{-1} when $\epsilon = 1$, 4, and 40, respectively). Note that also in this case the endergonicity of the **15** → **16** step is influenced by the H bonds formed in **15** between butylammonium and CN groups, which are lost in **16**. Moreover, **15**, which is characterized by a significant charge polarization due to the presence of the positively charged ammonium moiety, is more stabilized than **16** in a strongly polar environment.

In summary, H$_2$ formation and release can take place also according to a reaction pathway that implies the initial formation of a μ-H $Fe^{II}-Fe^{II}$ species, one-electron reduction, further protonation of Fe2, and H$_2$ release from an $Fe^{II}-Fe^{I}$ species.

It is worth noting that, after protonation of the Fe−Fe bond and monoelectron reduction, leading to the μ-H species [(μ-H)Fe$_2$DTMA(CO)$_3$(CN)$_2$CH$_3$S]$^{3-}$, further protonation of the *isolated* cluster should take place first on the CN groups and then on butylamine. Therefore, also in this case we have investigated the H$_2$ formation step on an $Fe^{II}-Fe^{I}$ complex, which differs from **13** for the protonation state of the two CN groups (**13′**; structure not shown), leading to **14′**, which is the doubly protonated homologue of **14**. It turns out that the ΔG value associated with the **13′** → **14′** step becomes more endergonic ($\Delta G = -1.3$, +3.9, and +6.9 kcal mol^{-1} when $\epsilon = 1$, 4, and 40, respectively) than that for the homologous step **13** → **14**, whereas the corresponding activation barrier (**13′** → **TS13-14′**) does not change significantly ($\Delta G^{\ddagger} = 0.8$, 4.6, and 6.9 kcal mol^{-1} when $\epsilon = 1$, 4, and 40, respectively).

H$_2$ Oxidation on Fe1. The results presented in the previous sections can also be analyzed and discussed considering the H$_2$ oxidation reaction, i.e., H$_2$ → 2e$^-$ + 2H$^+$. Indeed, the reaction pathway for H$_2$ oxidation could simply be described as the reverse of the steps discussed for H$_2$ formation. However, this has not to be necessarily valid for hydrogenases, as was recently underlined by Armstrong and co-workers, who noted that H$_2$ oxidation and H$^+$ reduction might imply different catalytic cycles.[38]

(38) Léger, C.; Jones, A. K.; Roseboom, W.; Albracht, S. P. J.; Armstrong, F. A. *Biochemistry* **2002**, *41*, 15736.

H$_2$ binding to the metal cluster is assumed to be the first key step in H$_2$ oxidation. In fact, it was previously shown that H$_2$ binding does not take place on an $Fe^{II}-Fe^{II}$ species because H$_2$ cannot displace the O-containing ligand (H$_2$O or a OH$^-$ ion) tightly bound to the oxidized form of the Fe$_2$S$_3$ cluster.[11,13,15]

H$_2$ binding to the Fe1 atom of the $Fe^{II}-Fe^{I}$ form of the Fe$_2$S$_3$ cluster (**6** + H$_2$ → **5**; Figure 2) is endergonic by 13.6, 12.8, and 12.2 kcal mol^{-1} when $\epsilon = 1$, 4, and 40, respectively). As expected, a significant contribution (up to 10 kcal mol^{-1}) to the endergonicity comes from the unfavorable entropy term due to the diminished rototranslational freedom of H$_2$.[32] It should be noted that the entropy effect could be partially overcome in the enzyme as a result of favorable enthalpy contributions in the H$_2$ uptake process mediated by the protein matrix.

According to our results, H$_2$ cleavage on the $Fe^{II}-Fe^{I}$ species **5** cannot take place because the product in which a H atom is coordinated to Fe1 and a H$^+$ is transferred to DTMA does not correspond to an energy minimum. Monoelectron oxidation of the $Fe^{II}-Fe^{I}$ species **5** leads to the $Fe^{II}-Fe^{II}$ species **4**, where H$_2$ cleavage (**4** → **3**) is exergonic when $\epsilon \geq 4$ ($\Delta G = +4.4$, -2.6, and -7.7 kcal mol^{-1} when $\epsilon = 1$, 4, and 40, respectively) and it is characterized by a small activation barrier ($\Delta G^{\ddagger} = 4.5$, 0.1, and 0.1 kcal mol^{-1} when $\epsilon = 1$, 4, and 40, respectively), in agreement with results previously reported by Fan and Hall.[12] The protonated DTMA ligand in complex **3** can lose a H$^+$ atom, leading to the $Fe^{II}-Fe^{II}$ species **2**, in which the H ion can be transferred from Fe1 to the amino group of DTMA, leading to the $Fe^{I}-Fe^{I}$ species **1**. However, the latter step is characterized by unfavorable ΔG (15.6, 9.5, and 4.7 kcal mol^{-1} when $\epsilon = 1$, 4, and 40, respectively) and $\Delta G^{\ddagger}$ values (18.4, 10.6, and 5.4 kcal mol^{-1} when $\epsilon = 1$, 4, and 40, respectively). On the other hand, if the $Fe^{II}-Fe^{II}$ complex **2** can undergo monoelectron oxidation, the H-atom transfer taking place on the resulting $Fe^{II}-Fe^{III}$ species **8** (leading to **7**) becomes thermodynamically less disfavored ($\Delta G = 11.2$, 4.7, and 0.0 kcal mol^{-1} when $\epsilon = 1$, 4, and 40, respectively). However, H$^+$ transfer from Fe1 to DTMA is still characterized by large free-energy barriers ($\Delta G^{\ddagger} = 19.1$, 16.3, and 14.5 kcal mol^{-1} when $\epsilon = 1$, 4, and 40, respectively),
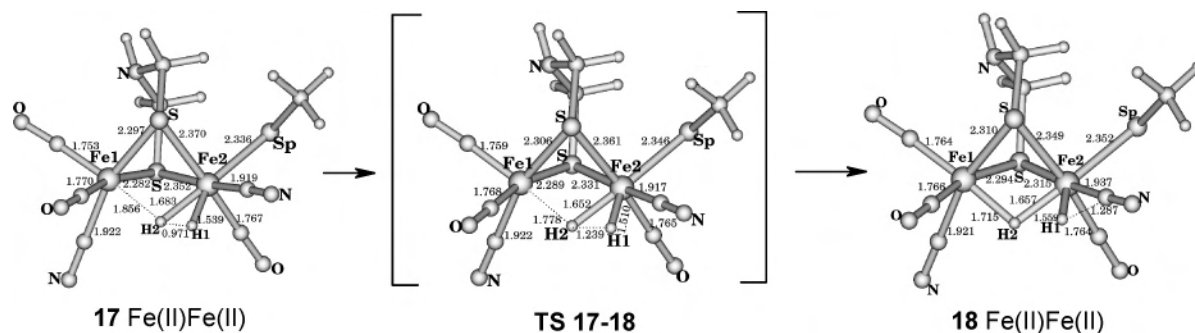
Figure 8. DFT structures (and formal oxidation states) of intermediates and transition states (in brackets) of species relevant to H$_2$ activation according to the reaction path b (see Scheme 1).

indicating that H$^+$ release from the cluster is the step characterized by the highest energy barrier in the H$_2$ cleavage reaction.

H$_2$ Oxidation on Fe2. In light of previous experimental[6] and theoretical[10] data highlighting a possible equilibrium between μ-CO and terminal CO species, it is conceivable that H$_2$ binding and activation might involve both Fe centers. Indeed, the Fe^{II}−Fe^I H$_2$−Fe2 adduct is stable (**14**; Figure 6), whereas H$_2$ cannot bind to Fe1 in an Fe^{II}−Fe^I isomer where all CO groups are terminally coordinated. Notably, H$_2$ binding to Fe2 in the Fe^{II}−Fe^I redox state is endergonic ($\Delta G = 17.5$, 20.7, and 22.9 kcal mol^{-1} when $\epsilon = 1$, 4, and 40, respectively), and it is more disfavored than H$_2$ binding to Fe1 in the corresponding μ-CO form (complex **5**; see above).

H$_2$ cleavage on the Fe^{II}−Fe^I form **14**, mediated by the amino group of the butylamine residue (**14** → **TS13-14** → **13**), is characterized by ΔG values equal to $+13.1$, $+3.1$, and -1.5 kcal mol^{-1} when $\epsilon = 1$, 4, and 40, respectively. The corresponding free-energy barriers are 16.7, 10.9, and 8.2 kcal mol^{-1}. Previous oxidation to an Fe^{II}−Fe^{II} H$_2$ complex (**12**; Figure 6) leads to a more favored H$_2$ cleavage step (**12** → **TS12-11** → **11**). In particular, the conversion from **12** to **11** is strongly exergonic ($\Delta G = -14.8$, -18.0, and -20.5 kcal mol^{-1} when $\epsilon = 1$, 4, and 40, respectively) and almost barrierless ($\Delta G^{\ddagger} < 0.5$ kcal mol^{-1}).

To better investigate the role of the external acid/base residue in the H$_2$ cleavage step, we have also studied the reactivity of the Fe^{II}−Fe^{II} H$_2$−Fe2S$_3$ complex, in which the lysine side-chain model has been removed (**17**; Figure 8). In **17**, the H$_2$ molecule is already strongly activated (H−H distance = 0.971 Å) and one of the H atoms interacts also with Fe1. Notably, also an isomer of the H$_2$ adduct in which the H$_2$ molecule is cleaved (H−H distance = 1.611 Å) corresponds to an energy minimum (**18**; Figure 8). Isomers **17** and **18** differ in energy by less that 0.5 kcal mol^{-1}, and the free-energy barrier along the **17** → **18** pathway (**TS17-18**; Figure 8) is extremely low ($\Delta G^{\ddagger} = 0.1$, 0.2, and 0.4 kcal mol^{-1} when $\epsilon = 1$, 4, and 40, respectively). In light of these results, it can be concluded that H$_2$ activation can take place on the Fe^{II}−Fe^{II} state of the [2Fe]$_H$ model without the involvement of an external base. In other words, the external base plays its role in the H$^+$ extraction step instead of in the H$_2$ cleavage step. Indeed, the facile activation of the H$_2$ moiety when coordinated to Fe2 was first proposed by

Bruschi et al.,[16] and it has very recently found support from other theoretical studies.[39]

Deprotonation of the lysine side-chain model in **11** leads to **10** (Figure 5), in which H$^+$ transfer from Fe2 to the amine group, leading to **9**, is thermodynamically and kinetically hindered ($\Delta G = 24.0$, 18.0, and 15.4 kcal mol^{-1} and $\Delta G^{\ddagger} = 25.1$, 21.5, and 20.0 kcal mol^{-1} when $\epsilon = 1$, 4, and 40, respectively). On the other hand, if **10** is oxidized to the corresponding Fe^{III}−Fe^{II} species **16**, the H$^+$ atom transfer to the amine residue becomes exergonic (**16** → **15**; $\Delta G = -2.9$, -6.2, and -7.1 kcal mol^{-1} when $\epsilon = 1$, 4, and 40, respectively) mainly because of the formation of strong H bonds in **15**. However, this step is still characterized by a large energy barrier ($\Delta G^{\ddagger} = 14.9$, 15.2, and 16.2 kcal mol^{-1} when $\epsilon = 1$, 4, and 40, respectively), confirming that the step corresponding to the second H$^+$ extraction from the *isolated* [2Fe]$_H$ cluster is characterized by the largest energy barriers in the H$_2$ cleavage pathway.

Conclusions

The analysis and comparison of the results obtained investigating H$^+$ reactivity on Fe^I−Fe^I models of the *isolated* [2Fe]$_H$ cluster indicate that H$_2$ formation can take place according to reaction pathways that imply initial protonation of the Fe^I−Fe^I form, leading to a formal Fe^{II}−Fe^{II} hydride species, subsequent monoelectron reduction to an Fe^{II}−Fe^I species, further protonation, and H$_2$ release. A comparison of pathways involving either the initial protonation of Fe1 or protonation of the Fe−Fe bond shows also that the former pathway is characterized by smaller activation barriers, as well as a downhill free-energy profile, suggesting that it could be the H$_2$ production pathway operative in the enzyme. However, initial H$^+$ binding to the Fe−Fe bond in the *isolated* [2Fe]$_H$ cluster is thermodynamically more favored than protonation of the Fe1 center. In this context, the investigation of the whole H cluster is predicted to be crucial to understanding to what extent the Fe$_4$S$_4$ cluster can influence the reactivity of the [2Fe]$_H$ cluster.

The pathway that implies the formation of μ-H Fe^{II}−Fe^{II} species is characterized by slightly larger barriers in the H$_2$ formation step. The latter observation can be relevant for the design of novel catalysts for H$^+$ reduction because it implies that even if the structure of the synthetic models does

(39) Zhou, T.; Mo, Y.; Zhou, Z.; Tsai, K. *Inorg. Chem.* **2005**, *44*, 4941.

Scheme 2. Plausible Catalytic Cycles for H$_2$ Oxidation and H$^+$ Reduction, As Deduced by DFT Calculations
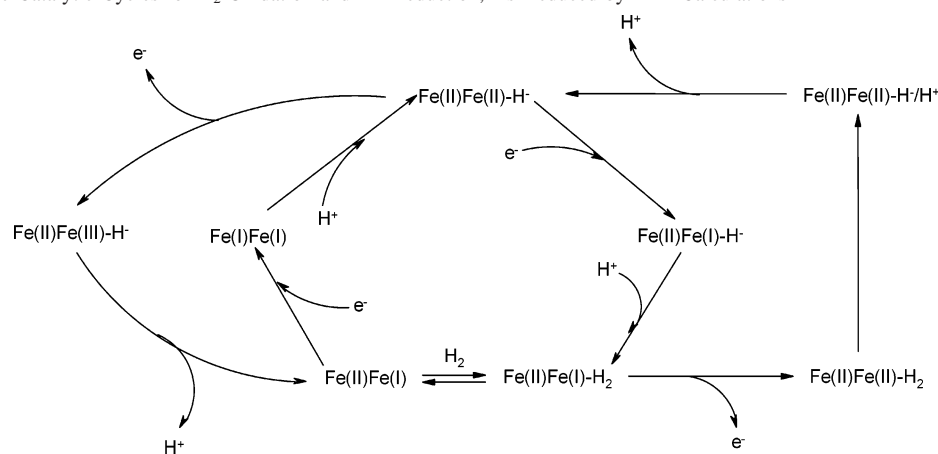
not resemble the structure of the [2Fe]$_H$ cluster in the enzyme, i.e., even if a CO group does not bridge the Fe centers, the bimetallic cluster can, nevertheless, be characterized by remarkable catalytic properties if H$_2$ formation takes place on an Fe^{II}–Fe^{II} species.

H$_2$ formation can take place quite easily also on an Fe^{II}–Fe^{II} species characterized by terminal coordination of H to Fe1 ($3 \rightarrow 4$; Figure 2), whereas it is strongly hindered on the corresponding μ-H Fe^{II}–Fe^{III} species ($11 \rightarrow 12$; Figure 6), in very good agreement with data recently reported by Rauchfuss and collaborators, showing that the Fe^{II}–Fe^{II} complex [Fe$_2$(edt)(μ-CO)(H)(CO)(PMe$_3$)$_4$]PF$_6$ reacts with Bronsted acids to give H$_2$, while isomeric μ-H compounds are nonreactive.[14]

H$_2$ cleavage can take place easily on Fe^{II}–Fe^{II} redox forms, in full agreement with previous results by Fan and Hall,[12] whereas it cannot take place or it is kinetically hindered on Fe^{II}–Fe^{I} species characterized by a μ-CO or all terminal CO groups, respectively. In particular, H$_2$ cleavage on an Fe^{II}–Fe^{II} form characterized by terminal CO groups does not need the involvement of an external base, which is only required to remove H$^+$ from the Fe$_2$S$_3$ cluster. Notably, the second H$^+$ extraction from the [2Fe]$_H$ cluster models is thermodynamically difficult on Fe^{II}–Fe^{II} species because the resulting

Fe^I–Fe^I forms are strong bases. Previous oxidation to Fe^{III}–Fe^{II} species makes the H$^+$ extraction from the cluster thermodynamically more favored. Moreover, in light of the present results, the extraction of the second H$^+$ from the cluster is proposed to correspond to the rate-limiting step in H$_2$ oxidation, both considering Fe^{II}–Fe^{II} and Fe^{II}–Fe^{III} species.

A comparison of H$_2$ oxidation and H$^+$ reduction pathways reveals also that the two reactions might follow different routes (Scheme 2). In particular, H$_2$ formation could involve only Fe^I–Fe^I, Fe^{II}–Fe^I, and Fe^{II}–Fe^{II} species, whereas in the H$_2$ cleavage catalytic cycle Fe^{III}–Fe^{II} species might be relevant.

Supporting Information Available: Computed CO and CN stretching frequencies for all computed intermediate species. This material is available free of charge via the Internet at http://pubs.acs.org.

IC051986M